Electronic structure and magnetism in $BaMn_2As_2$ and $BaMn_2Sb_2$

Jiming An
Materials Science and Technology Division, Oak Ridge National Laboratory, Oak Ridge, Tennessee 37831-6114, USA and Wuhan University of Technology, Wuhan 430070, China

A. S. Sefat, D. J. Singh, and Mao-Hua Du
Materials Science and Technology Division, Oak Ridge National Laboratory, Oak Ridge, Tennessee 37831-6114, USA

(Received 14 January 2009; revised manuscript received 2 February 2009; published 25 February 2009)

We study the properties of $ThCr_2Si_2$ structure $BaMn_2As_2$ and $BaMn_2Sb_2$ using density functional calculations of the electronic and magnetic properties as well as experimental measurements on single crystal samples of $BaMn_2As_2$. These materials are local moment magnets with moderate band gap antiferromagnetic semiconducting ground states. The electronic structures show substantial Mn-pnictogen hybridization, which stabilizes an intermediate spin configuration for the nominally d^5 Mn. The results are discussed in the context of possible thermoelectric applications and the relationship with the corresponding iron/cobalt/nickel compounds $Ba(Fe,Co,Ni)_2As_2$.

DOI: 10.1103/PhysRevB.79.075120 PACS number(s): 71.20.Lp, 72.15.Jf, 75.10.Lp

I. INTRODUCTION

Requirements for a thermoelectric material to be used in waste heat recovery include a high figure of merit, $ZT=\sigma S^2T/\kappa$, preferably unity or higher, and materials cost compatible with the application. Here S is the Seebeck coefficient (thermopower), σ is the electrical conductivity, and κ is the thermal conductivity. High ZT cannot be obtained without high thermopower.[1] Current materials for intermediate temperatures typical of requirements for automotive exhaust heat conversion contain substantial amounts of Te as in, e.g., PbTe. However, Te is a rare element whose supply is mainly as a byproduct of Cu production and whose cost is expected to sensitive to usage. In particular, this may lead to difficulties in applications that require large volumes of Te-based thermoelectric material. Therefore it is of interest to identify alternative materials based on common inexpensive elements. Among metals and metalloids these include alkaline earths (Mg,Ca,Sr,Ba), mid-3d transition elements, especially Mn and Fe and pnictogens (As,Sb). Wang *et al.*[2] recently reported measurements of the transport properties of single crystals of $BaMn_2Sb_2$ grown from Sn flux. They report a room temperature thermopower of $\sim 225\ \mu V/K$, but accompanied by a low electrical conductivity leading to low ZT. The conductivity increases with temperature, but this is accompanied by a decreasing thermopower. This suggests intrinsic semiconducting behavior, which is consistent with activated fits of the conductivity. Interestingly, a transition was found from a low activation energy of ~ 0.1 eV($T<470$ K) to a higher activation energy region (~ 1.1 eV) at $T>650$ K, possibly reflecting a crossover from an extrinsic to an intrinsic regime. However, doping studies have not yet been reported.

Recent discoveries of superconductivity[3,4] in $ThCr_2Si_2$ structure pnictides have led to renewed interest in this large class of compounds.[5,6] Among the compounds AM_2Pn_2, $A=Ca,Sr,Ba,Eu$, $Pn=As$, high temperature superconductivity is found for $M=Fe$, and an apparently different superconductivity for $M=Ni$.[7–9] The $M=Co$ compound, $BaCo_2As_2$, is near ferromagnetism,[10] while $CaCo_2P_2$ is reported as having ferromagnetically ordered Co planes, which are stacked antiferromagnetically.[11] Interestingly, unconventional superconductivity is found in $Ba(Fe_{1-x}Co_x)_2As_2$ for a substantial range of x around 0.1.[12] Turning to the electronic structures, the compounds with $M=Fe$, Co, and Ni show roughly similar shapes of their densities of states, with the main difference being the position of the Fermi energy, due to the different electron counts. These electronic structures show moderate hybridization between the transition metal d bands and the As p bands, with the main As p bands $\sim 2-3$ eV below the Fermi energy, E_F, and approximately $\sim 10-20\%$ As character in the d bands. Thus the As occurs nominally as As^{3-}. Interestingly, even though $ThCr_2Si_2$ is an very common structure type, the $Pn=Sb$ compounds, namely, $BaFe_2Sb_2$, $BaCo_2Sb_2$, and $BaNi_2Sb_2$, are not reported. On the other hand, the Mn compounds $BaMn_2P_2$, $BaMn_2As_2$, and $BaMn_2Sb_2$ are known phases. The corresponding Ca, Sr, and Eu materials are also known, although with structural distortions in some cases.[13–17]

From a practical point of view, there are several reports of remarkably high thermopowers accompanied by metallic conduction in the Fe-based superconducting phases.[18–22] These materials have relatively narrow manifolds of Fe d bands near the Fermi energy. These result from the combination of moderate Fe-As hybridization and expanded Fe-Fe distance as compared to bulk Fe. In any case, the values of S in the Fe compounds are too low by a factor of ~ 2 compared to practical thermoelectrics and are high at low temperatures, inapplicable to waste heat recovery. As mentioned, $BaMn_2Sb_2$ is reported to be a semiconductor.[2,17] We note that $BaMn_2Sb_2$, $BaMn_2As_2$, and $BaFe_2As_2$ are composed of common, inexpensive elements, which as mentioned is an important consideration for some thermoelectric applications. Key questions concern the relationship between $BaMn_2As_2$ and $BaMn_2Sb_2$ and that between the Mn and Fe compounds, as well as the related issue of whether the conductivity in the Mn compounds can be improved by doping, while at the same time maintaining high thermopowers.

II. THEORETICAL METHODS

The purpose of this paper is to further elucidate the electronic properties of these Mn compounds in relation to the Fe phases, in particular by comparing $BaMn_2As_2$ to $BaFe_2As_2$ and to $BaMn_2Sb_2$, which was recently studied by Xia *et al.*[17] We find that the Mn compounds are rather different from the Fe, Co, and Ni compounds in that there is much stronger hybridization with the pnictogen *p* states. This leads to an electronic structure that cannot be regarded as derived from that of the Fe compound with a different electron count. Furthermore, in contrast to the metallic character and itinerant magnetism in the Fe phases, we find local moment semiconducting behavior in both $BaMn_2Sb_2$ and $BaMn_2As_2$.

Electronic structure calculations were performed within density functional theory. We did calculations using both the local density approximation (LDA) and the generalized gradient approximation (GGA) of Perdew *et al.*,[23] and also using both the general potential linearized augmented plane wave (LAPW) method[24] similar to our earlier calculations for the Fe-based materials[25,26] and an ultrasoft pseudopotential method implemented in the QUANTUM ESPRESSO package.[27] For the LAPW calculations, we used two different codes, an in-house code and the WIEN2K code,[28] and compared results, finding no significant differences. We used LAPW sphere radii of 2.1 Bohr for the elements other than Ba in $BaMn_2As_2$ and 2.2 Bohr for all elements in $BaMn_2Sb_2$. Two different sphere radii were used for Ba in $BaMn_2As_2$: 2.35 Bohr with WIEN2K and 2.2 Bohr in the other LAPW calculations. In all cases, converged basis sets, corresponding to $R_{\min}k_{\max}=9$ with additional local orbitals[29] were used, where $R_{\min}$ is the minimum LAPW sphere radius and $k_{\max}$ is the plane wave cutoff. Convergence of the Brilloiun zone sampling was checked by directly calculating results using different grids. We used the literature values of the lattice parameters $a=4.418$ Å and $c=14.200$ Å for $BaMn_2Sb_2$ and $a=4.15$ Å and $c=13.47$ Å for $BaMn_2As_2$ with internal parameters z_{As} and z_{Sb} determined by LDA total energy minimization in the low energy antiferromagnetic state. The resulting values were $z_{Sb}=0.3594$ for $BaMn_2Sb_2$ and $z_{As}=0.3524$ for $BaMn_2As_2$. The value obtained for $BaMn_2Sb_2$ is in reasonable accord with the experimental value[17] of 0.3663.

Transport calculations were performed within the constant scattering time approximation using the BOLTZTRAP code.[30] For consistency we focus here on results obtained within the LDA with the LAPW method, but we note that the conclusions are robust with very similar results and conclusions emerging from the GGA plane wave calculations. We also note that our electronic structure for $BaMn_2Sb_2$ is quite similar to that reported previously by Xia *et al.*[17]

III. SYNTHESIS

Experimental characterization of $BaMn_2As_2$ was performed using single crystals. These were grown out of MnAs flux. The typical crystal sizes were $\sim 5\times 3\times 0.2$ mm^3. High purity elements (>99.9%) were used in the preparation of the samples. The source was Alfa Aesar. First, MnAs binary was prepared by placing mixtures of As and Mn pieces in a silica tube. These were reacted slowly by heating to 300 °C (25 °C/h, dwell 10 h) and to 600 °C (15 °C/h, dwell 75 h). Then a ratio of Ba:MnAs=1:5 was heated in an alumina crucible for 15 h at 1230 °C under partial atmosphere argon. This reaction was cooled at the rate of 2 °C/h, followed by decanting of the MnAs flux at 1120 °C.

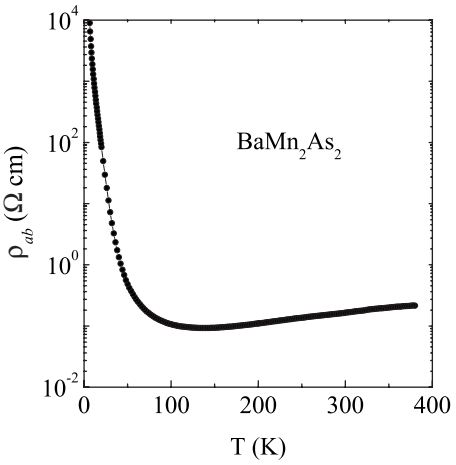

FIG. 1. Temperature dependence of the in-plane resistivity of $BaMn_2As_2$ between 1.8 and 380 K.

IV. CRYSTAL STRUCTURE, TRANSPORT, AND SPECIFIC HEAT

The crystals were malleable but well-formed plates with the [001] direction perpendicular to the large faces. The structural identification was made via powder x-ray diffraction using a Scintag XDS 2000 Θ-Θ diffractometer (Cu K_α radiation). The cell parameters were refined using least-squares fitting of the measured peak positions in the range $2\Theta=10°-90°$ using the Jade 6.1 MDI package. The resulting lattice parameters of $BaMn_2As_2$ were $a=4.1633(9)$ Å and $c=13.448(4)$ Å in the $ThCr_2Si_2$ structure ($I4/mmm$, $Z=2$). The cell volume for $BaMn_2As_2$ is then 233.087(4) Å^3, which is in accord with prior reports and much larger than $BaFe_2As_2$ [204.567(2) Å^3] (Ref. 12) or $BaCo_2As_2$ [197.784(1) Å^3] (Ref. 10).

Temperature dependent electrical resistivity measurements were performed on a Quantum Design physical property measurement system (PPMS), measured in the *ab* plane above 5 K. For $BaMn_2As_2$, the resistivity, ρ decreases with increasing temperature up to ~150 K, above which it gives a decreasing, metalliclike dependence (Fig. 1). The resistivity at room temperature is 165 mΩ cm. Unfortunately the crystals were too small for thermopower measurements.

Specific heat data, $C_p(T)$, were also obtained using the PPMS via the relaxation method. Figure 2 gives the temperature dependence of the specific heat. There are no features suggesting a phase transition in the specific heat up to 200 K. Below ~6 K, C/T has a linear T^2 dependence (inset of Fig. 2). The fitted Sommerfeld coefficient, $\gamma=0.79(2)$ mJ/(K^2 mol) or ~0.4 mJ/(K^2 mol Mn), is near zero. For comparison the value for $BaFe_2As_2$, which has a spin density wave instability gapping most of the Fermi sur-

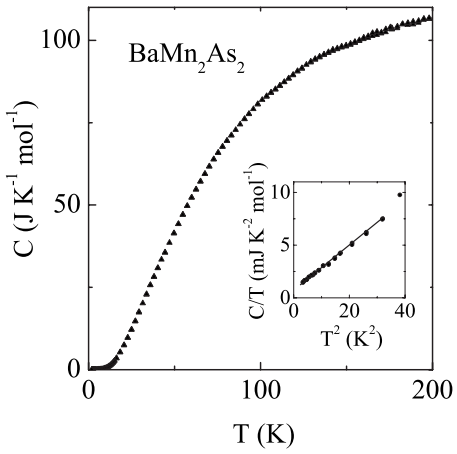

FIG. 2. Temperature dependence of the specific heat for $BaMn_2As_2$. Inset shows C/T vs T^2 and a linear fit between 1.8 and 3.5 K

face is 3.0 mJ/(K^2 mol Fe),[12] and the value for $BaCo_2As_2$ is 20.8 mJ/(K^2 mol Co).[10] In fact, it is likely that the small observed γ arises from a small amount of MnAs flux included in the sample and is therefore not intrinsic to $BaMn_2As_2$. This is based on squid measurements, where we find a small signal at 310 K, corresponding to the ordering temperature of MnAs. The value for the Debye temperature is $\Theta_D \sim 280$ K, estimated above 150 K, using the calculated values of the T/Θ_D dependence of the Debye specific heat model. Thus our transport and specific heat measurements are consistent with a small band gap semiconductor. They are not consistent with either a large gap insulator (e.g., a Mott insulator) or a metal with significant carrier density.

V. ELECTRONIC STRUCTURE AND MAGNETISM

We begin the discussion of the density functional investigation with a summary of our calculated results for $BaMn_2Sb_2$, which as mentioned are similar to those obtained previously by Xia *et al.*,[17] although in general the LAPW method is more accurate than the linear muffin tin orbital method employed in that work. Calculations were performed for a checkerboard antiferromagnetic ordering (AF-C), which is the lowest energy state, as well as a ferromagnetic ordering (F), and zone boundary antiferromagnetic orders alternating chains of like spin Mn (as in the spin density wave state of $BaFe_2As_2$) and a non-spin-polarized (NSP) case. The two cells with chain ordering are denoted AF-S1, which consists of chains stacked antiferromagnetically along the *c*-axis direction, and AF-S2, with ferromagnetic stacking. The energetics are summarized along with those of $BaMn_2As_2$ in Table I. We find a strong tendency toward moment formation, which results from the strong Hund's rule coupling on the nominal Mn^{2+} ions in the compound, with stable moments independent of the magnetic order. Integrating within the Mn LAPW sphere (radius 2.2 Bohr) we obtain moments of $3.47\mu_B$ for the F ordering and $3.55\mu_B$ for the *G*-type checkerboard AF-C ordering, which is the lowest energy state (n.b. *G*-type ordering is the experimental ground state at least for the phosphide).[16] Including contributions from all atoms in the unit cell, the F ordered spin magnetization is $3.76\mu_B$ on a per Mn basis, reflecting a small parallel contribution from the Sb. Significantly, this is considerably reduced from the nominal $5\mu_B$ expected for high spin Mn^{2+}. This reduction reflects strong hybridization between Mn *d* and Sb *p* states in this compound. In general, very strong hybridization is needed to effectively compete against the very strong Hund's interaction in the half-filled *d* shell of Mn^{2+} though we note that strong hybridization was previously identified in the phosphides by Hoffmann and Zheng[31,32] and by Gustenau *et al.*[33] Also, associated with the strong hybridization we find a very large energy difference between the ferromagnetic and antiferromagnetic orderings. This amounts to more than 0.29 eV/Mn in the LDA and implies a very high magnetic ordering temperature well above room temperature. This would be similar to the phosphide, which is reported to have an ordering temperature above 750K.[16] For comparison the corresponding energy for bcc Fe (Curie temperature, T_C=1043 K) is 0.4 eV, with opposite (ferromagnetic) sign.[34]

TABLE I. Magnetic energies in eV of $BaMn_2Sb_2$ and $BaMn_2As_2$ as obtained within the LDA on a per formula unit (two Mn) basis. The non-spin-polarized case, denoted NSP, is set as zero. F denotes ferromagnetic order, while AF-C is the checkerboard *G*-type antiferromagnetic ordering, and AF-S1 and AF-S2 are stripelike orders (see text).

	$BaMn_2Sb_2$	$BaMn_2As_2$
NSP	0	0
F	−1.55	−0.66
AF-S1	−1.94	−1.03
AF-S2	−1.91	−1.01
AF-C	−2.14	−1.32

In fact, strong, spin dependent hybridization is seen in the electronic structure, represented by the electronic density of states and projections (Fig. 3). As may be noted, the antiferromagnetic structure is found to be a small band gap semiconductor, E_g=0.21 eV in the LDA. The majority spin Mn *d* states overlap in energy with the Sb *p* states and are strongly mixed with them. The minority spin Mn *d* states are above the main Sb *p* DOS and are therefore less strongly mixed with the Sb states. Nonetheless, there is sufficient minority spin Mn *d*-Sb *p* hybridization to lead to noticeable Mn *d* character in the occupied valence band states. This is the main source of the moment reduction, corresponding to a Mn *d* electron count closer to Mn^{1+} than Mn^{2+}. Finally we note that such strong spin dependent hybridization while leading to strong superexchange interactions is highly unfavorable for carrier mobility in an antiferromagnet,[35] since at low *T* hopping between nearest neighbor sites with opposite spin will be suppressed and at higher *T* spin disorder will lead to strong scattering.

We now discuss our experimental and calculated results for $BaMn_2As_2$. The calculated magnetic energies (Table I) show strong local moment magnetism with a large exchange, similar to $BaMn_2Sb_2$, with the exception that the energies of

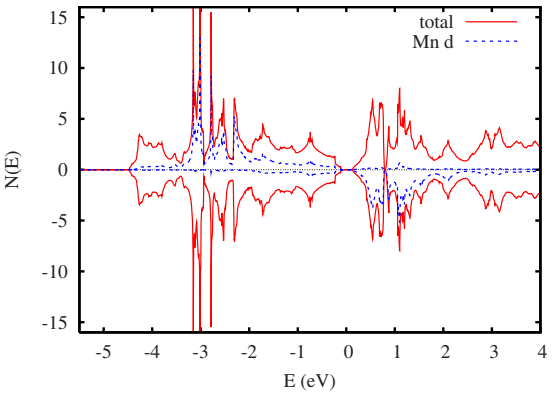

FIG. 3. (Color online) Electronic DOS and projections onto the LAPW spheres for antiferromagnetic $BaMn_2Sb_2$. Plot shows the total DOS above and below the axis, the Mn majority spin projection above and the Mn minority spin projection below. The remaining (non-Mn) contribution to the valence bands is mainly from Sb *p* states.

the magnetically ordered states are not as low compared to the non-spin-polarized case, as those in the antimonide. This reflects lower moments due to even stronger hybridization. The LDA total spin magnetization for the F ordering is $2.9\mu_B$/Mn, i.e., $\sim 0.9\mu_B$ lower than in the antimonide. The moment inside the 2.1 Bohr LAPW sphere is $3.20\mu_B$ for the AF ordering and $2.74\mu_B$ for the F ordering. Nonetheless, the ordering energy remains very high, again reflecting strong spin-dependent hybridization. The energy difference between the AF and F orderings is 0.33 eV/Mn in the LDA. The corresponding GGA value of 0.38 eV is similar; the main difference between the LDA and GGA results being that the moment formation is stronger in the GGA, leading to moments in the LAPW spheres of $3.07\mu_B$ for F ordering and $3.35\mu_B$ for AF ordering. Turning to the AF-S1 and AF-S2 orders, the energies are slightly lower than the average of the F and AF-C states. A simple nearest and next nearest neighbor superexchange picture is probably an oversimplification for these narrow gap semiconductors. However, the results indicate that the nearest neighbor interaction is dominant over further interactions and that the *c*-axis interaction is considerably weaker than the in-plane interaction and that it is antiferromagnetic.

The calculated LDA electronic density of states of $BaMn_2As_2$ is shown in Fig. 4 for both F and AF orderings. The low energy AF state again has a small semiconducting gap of 0.1 eV in the LDA and 0.2 eV in our GGA calculations. These low values are consistent with the activation energies from resistivity data below 470 K obtained by Wang *et al.*[2] Thus we interpret their low temperature value of ~ 0.1 eV as the intrinsic bulk gap for the AF ordered state. Within this scenario, the larger activation gap at high *T* would be associated with Anderson localization arising from magnetic disorder above the AF ordering temperature.

Strong spin-dependent hybridization is seen and in particular there is even more minority spin Mn character mixed with the pnictogen derived valence bands than in the antimonide. This stronger hybridization is consistent with the general trend that As has a greater tendency toward bond

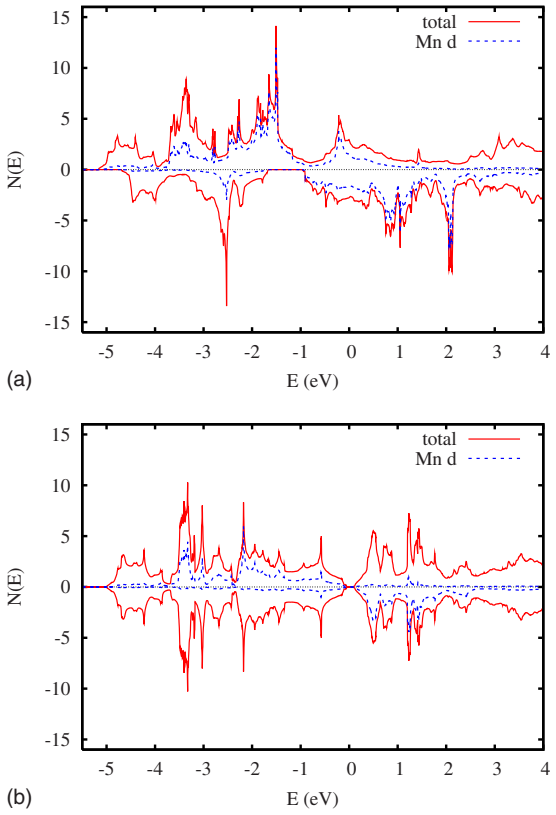

FIG. 4. (Color online) Electronic DOS and projections onto the LAPW spheres for ferromagnetic ordered (top) and antiferromagnetic $BaMn_2As_2$ (bottom). Plots show majority spin above the axis and minority spin below. The remaining (non-Mn) contribution to the valence bands is mainly from As *p* states.

formation with transition elements than Sb and is reflected in the higher energy difference between the F and AF magnetic orderings in $BaMn_2As_2$ than in $BaMn_2Sb_2$. We emphasize that this behavior is very different from that found in $BaFe_2As_2$, $BaCo_2As_2$, and $BaNi_2As_2$, which have some *d*-*p* hybridization, as in an oxide, but are much more ionic.[9,10,26] The distinct Mn-As bonding in this structure also explains why Mn is not an effective dopant for the Fe-based superconducting compounds, while Co and Ni are.[36]

VI. THERMOPOWER

As noted, antiferromagnetism with strong spin dependent hybridization is not favorable for high mobility conduction. Nonetheless, the chemical flexibility of the $ThCr_2Si_2$ structure suggests that high doping levels may be achievable. In that case, if the thermopower remains high, as in the oxide thermoelectric Na_xCoO_2, high *ZT* may result in spite of low mobility.[37]

Therefore we calculated the Seebeck coefficients from the LDA band structure as a function of doping level and temperature in the constant scattering time approximation. The results are shown in Figs. 5 and 6. As may be seen, high values consistent with reported data[2] for $BaMn_2Sb_2$ are obtained for modest doping. It would be of interest to compare to the experimental doping dependent thermopower for

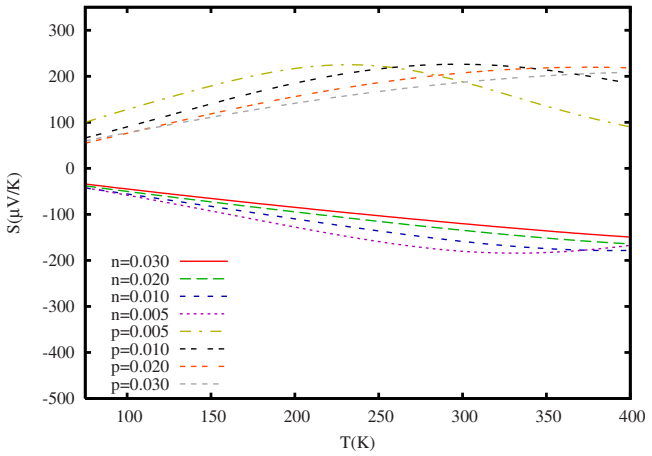

FIG. 5. (Color online) LDA constant scattering time approximation Seebeck coefficient in the basal plane of AF ordered $BaMn_2As_2$. The doping levels are in carriers per formula unit (2 Mn).

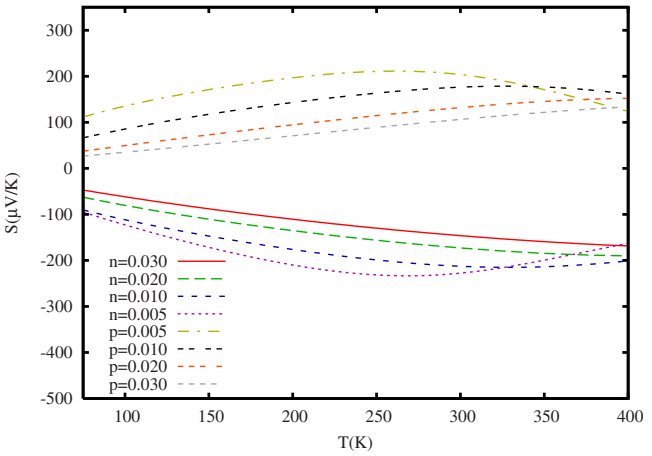

FIG. 6. (Color online) LDA constant scattering time approximation c-axis Seebeck coefficient of AF ordered $BaMn_2As_2$. The doping levels are in carriers per formula unit.

$BaMn_2As_2$. However, as mentioned, our crystals are too small for reliable thermopower measurements. The anisotropies are different for the valence and conduction bands. In the basal plane, the hole doping yields higher S than electron doping, while an opposite trend is found in the conduction bands. This difference is due to different band anisotropies. The constant scattering time transport anisotropy σ_{zz}/σ_{xx} estimated from the band anisotropy is 1.9 for the valence bands (p-type doping) and 0.5 for the conduction bands (n type). These modest anisotropies mean that the material is effectively a three dimensional intermetallic compound rather than a quasi-two-dimensional (quasi-2D) system. Turning to the values of S we observe that high values compatible with high ZT are only found for modest doping levels and not for high metallic doping levels such as those in Na_xCoO_2 (0.01 carriers per formula unit is 8.6×10^{19} cm^{-3}; the carrier concentration in thermoelectric Na_xCoO_2 is more than 1 order of magnitude higher).[38] Considering the likelihood of carrier localization in this magnetic material, this would initially seem not favorable for application of $BaMn_2As_2$ as a thermoelectric for waste heat recovery.

VII. SUMMARY AND CONCLUSIONS

To summarize, we characterize $BaMn_2As_2$ and $BaMn_2Sb_2$ as small band gap local moment antiferromagnetic semiconductors. We find a very strong spin dependent hybridization. This leads to high exchange energies, which are consistent with high magnetic ordering temperatures. The lowest energy state found is the G-type checkerboard antiferromagnetic state for both compounds. We note that the bonding, electronic structure, and magnetic properties are very distinct from those of the corresponding Fe, Co, and Ni compounds, which may explain why Mn leads to carrier localization rather than effective doping in $BaFe_2As_2$ and related materials.

The strong spin dependent hybridization is not favorable for high carrier mobility. Nonetheless, the high thermopowers do suggest that experimental doping studies should be performed to determine the maximum ZT in this material.

ACKNOWLEDGMENTS

We are grateful for helpful discussions with B. C. Sales and D. Mandrus. This work was supported by the Department of Energy, through the Division of Materials Sciences and Engineering, the Vehicle Technologies, Propulsion Materials Program and the ORNL LDRD program.

[1] This is because of the electronic contribution to thermal conductivity. In materials where the Wiedemann-Franz relation $\kappa_e = L\sigma T$ holds, it can be shown that $ZT>1$ requires $S > 160$ μV/K.

[2] H. F. Wang, K. F. Cai, H. Li, L. Wang, and C. W. Zhou, J. Alloys Compd. (to be published 2008).

[3] Y. Kamihara, T. Watanabe, M. Hirano, and H. Hosono, J. Am. Chem. Soc. **130**, 3296 (2008).

[4] M. Rotter, M. Tegel, and D. Johrendt, Phys. Rev. Lett. **101**, 107006 (2008).

[5] W. B. Pearson and P. Villars, J. Less-Common Met. **97**, 119 (1984); **97**, 133 (1984).

[6] G. Just and P. Paufler, J. Alloys Compd. **232**, 1 (1996).

[7] F. Ronning, N. Kurita, E. D. Bauer, B. L. Scott, T. Park, T. Klimczuk, R. Movshovich, and J. D. Thompson, J. Phys.: Condens. Matter **20**, 342203 (2008).

[8] N. Kurita, F. Ronning, Y. Tokiwa, E. D. Bauer, A. Subedi, D. J. Singh, J. D. Thompson, and R. Movshovich, arXiv:0811.3426 (unpublished).

[9] A. Subedi and D. J. Singh, Phys. Rev. B **78**, 132511 (2008).

[10] A. S. Sefat, D. J. Singh, R. Jin, M. A. McGuire, B. C. Sales, and D. Mandrus, Phys. Rev. B **79**, 024512 (2009)
[11] M. Reehuis, W. Jeitschko, G. Kotzba, B. Zimmer, and X. Hu, J. Alloys Compd. **266**, 54 (1998).
[12] A. S. Sefat, R. Jin, M. A. McGuire, B. C. Sales, D. J. Singh, and D. Mandrus, Phys. Rev. Lett. **101**, 117004 (2008).
[13] E. Brechtel, G. Cordier, and H. Schafer, Z. Naturforsch. B **34B**, 921 (1979).
[14] A. C. Payne, A. E. Sprauve, M. M. Olmstead, S. M. Kauzlarich, J. Y. Chan, B. A. Reisner, and J. W. Lynn, J. Solid State Chem. **163**, 498 (2002).
[15] S. Bobev, J. Merz, A. Lima, V. Fritsch, J. D. Thompson, J. L. Sarao, M. Gillessen, and R. Dronskowski, Inorg. Chem. **45**, 4047 (2006).
[16] S. L. Brock, J. E. Greedan, and S. M. Kauzlarich, J. Solid State Chem. **113**, 303 (1994).
[17] S. Q. Xia, C. Myers, and S. Bobev, Eur. J. Inorg. Chem. **2008**, 4262 (2008).
[18] A. S. Sefat, M. A. McGuire, B. C. Sales, R. Y. Jin, J. Y. Howe, and D. Mandrus, Phys. Rev. B **77**, 174503 (2008).
[19] L. Pinsard-Gaudart, D. Berardan, J. Bobroff, and N. Dragoe, Phys. Status Solidi (RRL) **2**, 185 (2008).
[20] M. A. McGuire, A. C. Christianson, A. S. Sefat, B. C. Sales, M. D. Lumsden, R. Y. Jin, E. A. Payzant, D. Mandrus, Y. B. Luan, V. Keppens, V. Varadarajan, J. W. Brill, R. P. Hermann, M. T. Sougrati, F. Grandjean, and G. J. Long, Phys. Rev. B **78**, 094517 (2008).
[21] L. J. Li, Y. K. Li, Z. Ren, Y. K. Luo, X. Lin, M. He, Q. Tao, Z. W. Zhu, G. H. Cao, and Z. A. Xu, Phys. Rev. B **78**, 132506 (2008).
[22] L. J. Li, Y. K. Luo, Q. B. Wang, H. Chen, Z. Ren, Q. Tao, Y. K. Li, X. Lin, M. He, Z. W. Zhu, G. H. Cao, and Z. A. Xu, arXiv:0809.2009 (unpublished).
[23] J. P. Perdew, K. Burke, and M. Ernzerhof, Phys. Rev. Lett. **77**, 3865 (1996).
[24] D. J. Singh and L. Nordstrom, *Planewaves Pseudopotentials and the LAPW Method*, 2nd ed. (Springer, Berlin, 2006).
[25] D. J. Singh and M. H. Du, Phys. Rev. Lett. **100**, 237003 (2008).
[26] D. J. Singh, Phys. Rev. B **78**, 094511 (2008).
[27] P. Giannozzi *et al.*, http://www.quantum-espresso.org
[28] P. Blaha, K. Schwarz, G. Madsen, D. Kvasnicka, and J. Luitz, http://www.wien2k.at
[29] D. Singh, Phys. Rev. B **43**, 6388 (1991).
[30] G. K. H. Madsen and D. J. Singh, Comput. Phys. Commun. **175**, 67 (2006).
[31] R. Hoffmann and C. Zheng, J. Phys. Chem. **89**, 4175 (1985).
[32] C. Zheng and R. Hoffmann, J. Solid State Chem. **72**, 58 (1988).
[33] E. Gustenau, P. Herzig, and A. Neckel, J. Alloys Compd. **262-263**, 516 (1997).
[34] D. J. Singh, Phys. Rev. B **45**, 2258 (1992).
[35] P. W. Anderson, Phys. Rev. **115**, 2 (1959).
[36] S. Matsuishi, Y. Inoue, T. Nomura, Y. Kamihara, M. Hirano, and H. Hosono, arXiv:0811.1147 (unpublished).
[37] I. Terasaki, Y. Sasago, and K. Uchinokura, Phys. Rev. B **56**, R12685 (1997).
[38] Our calculated thermopowers based on the GGA electronic structure are similar except that the values at high temperatures and low doping levels are larger owing the larger GGA gap, which leads to less minority carrier conduction.